

N. Nagendra*, CH. Amanulla, M. Sudhakar Reddy, and V. Ramachandra Prasad

Hydromagnetic Flow of Heat and Mass Transfer in a Nano Williamson Fluid Past a Vertical Plate With Thermal and Momentum Slip Effects: Numerical Study

<https://doi.org/10.1515/nleng-2017-0057>

Received May 9, 2017; revised February 2, 2018; accepted April 19, 2018.

Abstract: In this article, the study of heat, momentum and mass (species) transfer in an electro-conductive polymer on the external surface of a vertical plate. The effects of Brownian motion and thermophoresis are incorporated in the model in the presence of both heat and nanoparticle mass transfer convective conditions. The Williamson viscoelastic model is employed which is representative of certain industrial polymers. The non-dimensional, transformed boundary layer equations for momentum and energy are solved with the second order accurate implicit Keller box finite difference method under appropriate boundary conditions. The influence of Weissenberg number, magnetic body force parameter, thermal slip parameter, hydrodynamic slip parameter, stream wise variable and Prandtl number on thermo fluid characteristics are presented graphically and discussed. A weak elevation in temperature accompanies increasing Weissenberg number whereas a significant acceleration in the flow is computed near the plate surface. Rate of heat transfer is reduced with increases the Weissenberg number. The study is relevant to enrobing processes for electric-conductive nano-materials, of potential use in aerospace, smart coating transport phenomena and other industries.

Keywords: Nanoparticles; Magnetic nanofluid; Species diffusion; Steady flow; Williamson model; Thermal convection; thermal and momentum slip

***Corresponding Author: N. Nagendra**, Department of Mathematics, Madanapalle Institute of Technology and Science, Madanapalle-517325, India, E-mail: nagsvu76@gmail.com

CH. Amanulla, M. Sudhakar Reddy, Department of Mathematics, Madanapalle Institute of Technology and Science, Madanapalle-517325, India

V. Ramachandra Prasad, School of Advanced Sciences, VIT University, Vellore- 600048, India

1 Introduction

Magnetohydrodynamic (MHD) boundary layers with heat and mass transfer over surfaces are found in many engineering and geophysical applications such as geothermal reservoirs, thermal insulation, enhanced oil recovery, packed-bed catalytic reactors, and cooling of nuclear reactors. Many chemical engineering processes like metallurgical and polymer extrusion processes involve cooling of a molten liquid being stretched into a cooling system. Some polymer liquids like polyethylene oxide and polyisobutylene solution in cetane, having better electromagnetic properties are normally used as cooling liquid as their flow can be regulated by external magnetic fields to improve the quality of the final product. As another application of the MHD flows in fluids and Nanofluids, we find the MHD flow in biomagnetic fluids (e.g., human blood), this topic is useful in different areas of bioengineering and medical sciences. The blood is a biological fluid, which has a magnetic behavior, it can be regarded as a suspension of magnetic particles (i.e., hemoglobin molecules) in non-Newtonian fluid (i.e., plasma). To view some recent works dealing with the Magnetohydrodynamic flow of blood, the reader is referred to [1–6] and the references therein. The properties of nanofluids need a lot of fine tuning, many seemingly contradicting studies need clarity and validation. Nanofluids have potential applications in micro-electronics, fuel cells, rocket propulsion, environmental de-toxification, spray coating of aircraft wings, pharmaceutical suspensions, medical sprays etc. These applications of nanofluids are largely attributable to the enhanced thermal conductivity and Brownian motion dynamics which can be exploited to immense benefit. Nanomaterials work efficiently as new energy materials since they incorporate suspended particles with size as the same as or smaller than the size of de Broglie wave [7]. The use of nanoparticles is now a subject of abundant studies, and aspects of particular interest are Brownian motion and thermophoretic transport. Nanofluids constitute

a new class of heat transfer fluids comprising a conventional base fluid and nano-particles. The nanoparticles are utilized to enhance the heat transfer performance of the base fluids [8]. The cooling rate requirements cannot be obtained by the ordinary heat transfer fluids because their thermal conductivity is not adequate. Brownian motion of the nanoparticles enhances the thermal conductivity of base fluids, although there may be many more mechanisms at work which exert a contribution. The concept of nanofluids was introduced by Choi [9] wherein he proposed the suspension of nanoparticles in a base fluid such as water, oil, and ethylene glycol. Buongiorno [10] attempted to explain the increase in the thermal conductivity of such fluids and developed a model that emphasized the key mechanisms in laminar flow as being particle Brownian motion and thermophoresis.

Furthermore the *non-Newtonian* properties of different nanofluid suspensions have also attracted interest in simulating rheological behavior with different models. Noghrehabadi *et al.* [11] investigated the effects of the slip boundary condition on the heat transfer characteristics for a stretching sheet subjected to convective heat transfer in the presence of nanoparticles. They found that the flow velocity and the surface shear stress on the stretching sheet are strongly influenced by the slip parameter with a decrease in the momentum boundary layer thickness and increase in thermal boundary layer thickness. Khan and Pop [12] studied the problem of laminar fluid flow which results from a stretching of a flat surface in a nanofluid. They analyzed the development of the steady boundary layer flow, heat transfer and nanoparticle volume fraction, observing that the reduced Nusselt number decreased while the reduced Sherwood number increased with greater volume fraction. Uddin *et al.* [13] analyzed anisotropic slip effects on nanofluid bioconvection boundary layers from a translating sheet. Uddin *et al.* [14] used a linear group similarity transformations with Maple software for numerical solutions for mixed convection slip flow from stretching sheet with nanoparticles. Many such studies have been communicated and have usually adopted the so-called “active control” boundary condition, based on the Kuznetsov-Nield formulation [15] for natural convective boundary layer flow of a nanofluid over a vertical surface featuring Brownian motion and thermophoresis. However Kuznetsov and Nield [16] re-visited their original model, refining this formulation with passive control of nanofluid particle fraction at the boundary rather than active control to be more physically realistic. This recent boundary condition provides one of the motivations for the present research.

The above studies considered the nanofluid to be *electrically non-conducting*. However new developments in magnetic nanofluids have emerged in recent years which require magnetohydrodynamics to simulate the response of nanofluids to applied magnetic fields. A number of researchers have simulated various types of multi-physical hydrodynamics problems of magnetic nanofluids in different configurations, using a diverse range of numerical methods. Both purely fluid flow and heat transfer from a cylinder to non-Newtonian fluids have been reported in a number of theoretical investigations. Malik *et al.* [17] used the Runge–Kutta Fehlberg method to obtain numerical solutions for steady thermal boundary layer flow of a Casson nanofluid flowing over a vertical radially exponentially-stretching cylinder. Ali *et al.* [18] have investigated analytically the unsteady MHD nanofluid flow over a vertical plate embedded in a porous medium with time dependent velocity, temperature and concentration, in the case where the presence of a chemical reaction and the effect of thermal radiation are taken into account governing equations. Mixed convective nanofluid in a lid-driven cavity flow solved with finite volume technique by Muthamilselvan and Doh [19]. Muthamilselvan and Kumar [20] used the finite volume method to explain the mixed convection heat transfer in a lid-driven cavity filled with nanofluid for different aspect ratios. The nanofluid boundary layer flow over a heated stretching sheet in the presence of unsteady free stream condition and thermal radiation is analysed by Das *et al.* [21]. The stagnation point flow of a nanofluid over a stretching/shrinking sheet in a porous medium with thermal radiation is considered by Pal *et al.* [22]. The hydromagnetic boundary layer flow of a nanofluid over a stretching sheet with Newtonian heating and dissipation effects is investigated by Mahatha *et al.* [23]. The unsteady hydromagnetic boundary-layer flow of a nanofluid over a horizontal stretching sheet in the presence of melting and heat generation or absorption effect is considered by Chamkha *et al.* [24]. The hydromagnetic boundary layer flow of a radiative nanofluid over a stretching sheet is analysed by Ferdows *et al.* [25] and concluded that the stretching parameter enhances the nanofluid temperature. Awad *et al.* [26] studied the unsteady Oldroyd-B Nanofluid flow over a stretching sheet. They found that the larger values of Deborah numbers are indicative that the Oldroyd-B nanofluid is stretched. The influence of multiple slips and viscous dissipation on boundary layer flow of a nanofluid over a stretching sheet in the presence of first order and chemical reaction is investigated by Ahmed [27]. He found that the corresponding slip parameters reduce the corresponding profiles.

These studies however did not consider the Williamson model. This is a shear-thinning non-Newtonian model which quite accurately simulates polymer viscoelastic flows over a wide spectrum of shear rates. In Williamson fluids the viscosity is reduced with rising shear stress rates. This model has found some popularity in engineering simulations. Prasannakumara *et al.* [28] used the Runge-Kutta-Fehlberg shooting algorithm to analyse reactive-radiative flow of Williamson viscoelastic nanofluid from a stretching sheet in a permeable material. Khan and Khan [29] investigated Blasius, Sakiadis, stretching and stagnation point flows of Williamson fluid using the homotopy analysis method, over a range of Weissenberg numbers. Bég *et al.* [30] presented extensive numerical solutions for hydromagnetic pumping of a Williamson fluid using a modified differential transform method, observing that a change in Weissenberg number strongly modifies the pressure difference and axial velocity. Further studies of transport phenomena in Williamson fluids include Rao and Rao [31] and Dapra and Scarpi [32]. Mabood *et al.* [33] reported MHD boundary layer flow and heat transfer of nanofluids over a heated stretching sheet. Kumar *et al.* [34] discussed the MHD Williamson nanofluid over an exponential stretching sheet with the effects of Thermal Radiation, Chemical Reaction and Porous Medium. Kho *et al.* [35] by considering the factor of MHD flow, mass and heat transfer analysis of Williamson nanofluid past over a stretching sheet.

In recent years with the development of hydrophobic surfaces, *slip flows* have garnered some attention in nanofluid dynamics. In several circumstances a simple direct linear correlation has been supposed where the proportionality portion is given by slip factor. The magnitude and direction of slip is a function of the wall shear stress which is related to the applied stress. Recently Amanulla *et al.* [36, 37] discussed the slip influence of MHD Williamson Nano fluid flow for different types of physical phenomena's. Uddin *et al.* [38] described slip effects on free convective MHD boundary layer flow of nanofluid over a moving plate. Uddin *et al.* [39, 40] investigated the steady magnetohydrodynamic laminar free convective boundary layer multiple slip flow of a nanofluid from a stretching/shrinking sheet and vertical plate through porous medium.

In the present investigation, we consider the *magnetohydrodynamic convection boundary layer flow of a Williamson nano polymeric fluid external to a vertical plate with slip conditions*. The present study employs a finite difference numerical method due to Keller for solving the two-dimensional steady flow and heat and mass transfer in a Williamson nano polymeric liquid boundary layer

from a plate. Verification of the computations is conducted for the special case of non-magnetic, Newtonian flow in the absence of Newtonian heating with earlier published literature. The study finds applications in electroconductive thermal polymer processing systems.

2 Magnetohydrodynamic Viscoelastic Slip Thermofluid Model

The regime under investigation is illustrated in Fig. 1. Steady, incompressible hydromagnetic Williamson non-Newtonian boundary layer flow and heat and mass transfer from a vertical body under radial magnetic field is considered. For an incompressible Williamson fluid, the continuity (mass conservation) and momentum equations are given as:

$$\operatorname{div}V = 0, \quad (1)$$

$$\rho \frac{dV}{dt} = \operatorname{div}S + \rho b, \quad (2)$$

where ρ the density of the fluid, V is the velocity vector, S is the Cauchy stress tensor, b represents the specific body force vector, and d/dt represents the material time derivative. The constitutive equations of the Williamson nanofluid model [33-37] are given as:

$$S = -pI + \tau \quad (3)$$

$$\tau = \left(\mu_{\infty} + \frac{(\mu_0 - \mu_{\infty})}{1 - \Gamma \dot{\gamma}} \right) A_1, \quad (4)$$

Here p is the pressure, I is the identity vector, τ is the extra stress tensor, μ_0 are the limiting viscosities at zero and at infinite shear rate, Γ is the time constant (>0), A_1 is the first Rivlin-Erickson tensor and $\dot{\gamma}$ is defined as follows:

$$\dot{\gamma} = \sqrt{\frac{1}{2}\pi}, \quad (5)$$

$$\pi = \operatorname{trace}(A_1^2) \quad (6)$$

Here we considered the case for which $\mu_{\infty} = 0$ and thus eq. (4) can be written as:

$$\tau = \left(\frac{\mu_0}{1 - \Gamma \dot{\gamma}} \right) A_1, \quad (7)$$

Or by using binomial expansion we get:

$$\tau = \mu_0 (1 + \Gamma \dot{\gamma}) A_1. \quad (8)$$

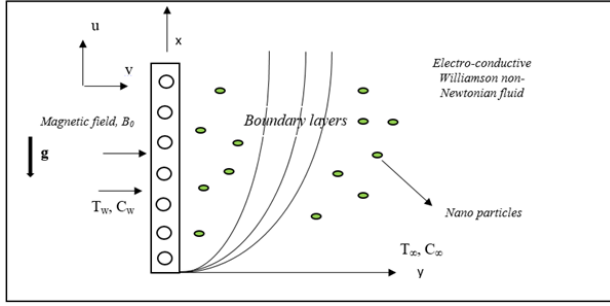


Fig. 1: Magnetohydrodynamic non-Newtonian heat transfer from a vertical plate

The two-dimensional mass, momentum and energy boundary layer equations governing the flow in an (x,y) coordinate system may be shown to take the form [33–37]:

$$\frac{\partial u}{\partial x} + \frac{\partial v}{\partial y} = 0 \quad (9)$$

$$u \frac{\partial u}{\partial x} + v \frac{\partial u}{\partial y} = \nu \frac{\partial^2 u}{\partial y^2} + \sqrt{2} \nu \Gamma \frac{\partial u}{\partial y} \frac{\partial^2 u}{\partial y^2} + g\beta(T - T_\infty) + g\beta^*(C - C_\infty) - \frac{\sigma B_0^2}{\rho} u \quad (10)$$

$$u \frac{\partial T}{\partial x} + v \frac{\partial T}{\partial y} = \alpha \frac{\partial^2 T}{\partial y^2} + \tau \left(D_B \frac{\partial C}{\partial y} \frac{\partial T}{\partial y} + \frac{D_T}{T_\infty} \left(\frac{\partial T}{\partial y} \right)^2 \right) \quad (11)$$

$$u \frac{\partial C}{\partial x} + v \frac{\partial C}{\partial y} = D_B \frac{\partial^2 C}{\partial y^2} + \frac{D_T}{T_\infty} \frac{\partial^2 T}{\partial y^2} \quad (12)$$

The boundary conditions for the considered flow with velocity and thermal slip are:

$$\text{At } y = 0, \quad u = N_0 \frac{\partial u}{\partial y}, \quad v = 0, \quad T = T_w + K_0 \frac{\partial T}{\partial y}, \quad C = C_w$$

$$\text{As } y \rightarrow \infty, \quad u \rightarrow 0, \quad v \rightarrow 0, \quad T \rightarrow T_\infty, \quad C \rightarrow C_\infty \quad (13)$$

Here N_0 is the velocity slip factor, K_0 is the thermal slip factor and T_∞ is the free stream temperature. For $N_0 = 0 = K_0$, one can recover the no-slip case. The stream function ψ is defined by $u = \frac{\partial \psi}{\partial y}$ and $v = -\frac{\partial \psi}{\partial x}$, and therefore, the continuity equation is automatically satisfied. In order to write the governing equations and the boundary conditions in dimensionless form, the following non-dimensional quantities are introduced:

$$\begin{aligned} \xi &= \frac{V_0 x}{\nu} (Gr_x)^{-1/4}, \quad \eta = \frac{y}{x} (Gr_x)^{1/4}, \\ \psi &= 4 \nu (Gr_x)^{1/4} \left(f(\xi, \eta) + \frac{1}{4} \xi \right), \\ \theta(\xi, \eta) &= \frac{T - T_\infty}{T_w - T_\infty}, \quad \phi(\xi, \eta) = \frac{C - C_\infty}{C_w - C_\infty}, \\ We &= \frac{4\sqrt{2}\nu\Gamma Gr_x^{3/4}}{x^2}, \quad Gr_x = \frac{g\beta(T_w - T_\infty)x^3}{4\nu^2} \end{aligned} \quad (14)$$

The emerging momentum and heat (energy) conservation equations in dimensionless form assume the following form:

$$\begin{aligned} f'''' + (3f + \xi)f'' - 2f'^2 + We f'' f'''' + \theta + N\phi - Mf' \\ = \xi \left(f' \frac{\partial f'}{\partial \xi} - f'' \frac{\partial f}{\partial \xi} \right) \end{aligned} \quad (15)$$

$$\frac{\theta''}{Pr} + (3f + \xi)\theta' + N_b \phi' \theta' + N_t \theta'^2 = \xi \left(f' \frac{\partial \theta}{\partial \xi} - \theta' \frac{\partial f}{\partial \xi} \right) \quad (16)$$

$$\frac{\phi''}{Le} + (3f + \xi)\phi' + \frac{1}{Le} \frac{N_b}{N_t} \theta'' = \xi \left(f' \frac{\partial \phi}{\partial \xi} - \phi' \frac{\partial f}{\partial \xi} \right) \quad (17)$$

The transformed dimensionless boundary conditions are reduced to:

$$\text{At } \eta = 0, \quad f = 0, \quad f' = S_f f''(0), \quad \theta = 1 + S_T \theta'(0), \quad \phi = 1$$

$$\text{As } \eta \rightarrow \infty, \quad f' \rightarrow 0, \quad \theta \rightarrow 0, \quad \phi \rightarrow 0 \quad (18)$$

where $S_f = N_0 Gr^{1/4}/x$ and $S_T = K_0 Gr^{1/4}/x$ are the non-dimensional velocity slip and thermal jump parameters, respectively, $Pr = \nu/\alpha$ is Prandtl number; $M = \sigma B_0^2 x^2/\nu\rho Gr^{1/2}$, $Le = \nu/D_B$ is the Lewis number; $Nt = (\rho c)_p D_T (T_w - T_\infty)/(\rho c)_f \nu T_\infty$ is the thermophoresis parameter; $Nb = (\rho c)_p D_B (C_w - C_\infty)/(\rho c)_f \nu$ is the Brownian motion parameter; $N = \beta^*(C_w - C_\infty)/\beta(T_w - T_\infty)$ is the concentration to thermal buoyancy ratio parameter. All other parameters are defined in the nomenclature.

The skin-friction coefficient (plate surface shear stress) and the local Nusselt number (plate surface heat transfer rate) can be defined, respectively, using the transformations described above with the following expressions:

$$\frac{1}{4} Gr_x^{-3/4} C_f = f''(\xi, 0) + \frac{We}{2} (f''(\xi, 0))^2 \quad (19)$$

$$Gr_x^{-1/4} Nu = -\theta'(\xi, 0) \quad (20)$$

$$Gr_x^{-1/4} Sh = -\phi'(\xi, 0) \quad (21)$$

3 Computational Solution With Keller Box Implicit Method

The transformed, nonlinear, multi-physical boundary value problem defined by Eqns. (15) - (17) can be solved via a number of numerical schemes. Here we implement

a popular, second order accurate implicit finite difference method originally developed by Keller [41]. Recent studies featuring this method in the context of magnetohydrodynamic and rheological flows include Amanulla *et al.* [42, 43] and Hydromagnetic Non-Newtonian Nanofluid slip boundary layer flows by Subba Rao *et al.* [44]. In the Keller box scheme, the multi-degree, multi-order coupled partial differential equations defined in (14) and (15) are first reduced to a system of first order equations. These equations are then discretized with the finite difference approximations with appropriate step lengths in each coordinate direction. Introducing the new variables:

$$f' = u \quad (22)$$

$$u' = v \quad (23)$$

$$\theta = s \quad (24)$$

$$s' = t \quad (25)$$

$$g' = p \quad (26)$$

Eqns. (15) - (17) reduce then to the form:

$$v' + 3fv + \xi v + Wevv' - 2u^2 + s + Ng - Mu = \xi \left(u \frac{\partial u}{\partial \xi} - v \frac{\partial f}{\partial \xi} \right) \quad (27)$$

$$\frac{t'}{Pr} + (3f + \xi)t + N_b \phi' t + N_t t^2 = \xi \left(u \frac{\partial s}{\partial \xi} - t \frac{\partial f}{\partial \xi} \right) \quad (28)$$

$$\frac{p'}{Le} + (3f + \xi)p + \frac{1}{Le} \frac{N_b}{N_t} t' = \xi \left(u \frac{\partial g}{\partial \xi} - p \frac{\partial f}{\partial \xi} \right) \quad (29)$$

where primes denote differentiation with respect to η .

In terms of the dependent variables, the boundary conditions (18) become:

$$\begin{aligned} \text{At } \eta = 0: & \quad u = 0, \quad f = 0, \quad s = 1, \quad g = 1 \\ \text{As } \eta \rightarrow \infty: & \quad u \rightarrow 0, \quad v \rightarrow 0, \quad s \rightarrow 0, \quad g \rightarrow 0 \end{aligned} \quad (30)$$

A two-dimensional computational mesh (grid) is imposed on the ξ - η plane as shown in Fig. 2. The stepping process is defined by:

$$\eta_0 = 0, \quad \eta_j = \eta_{j-1} + h_j, \quad j = 1, 2, \dots, J, \quad \eta_J \equiv \eta_\infty \quad (31)$$

$$\xi^0 = 0, \quad \xi^n = \xi^{n-1} + k_n, \quad n = 1, 2, \dots, N. \quad (32)$$

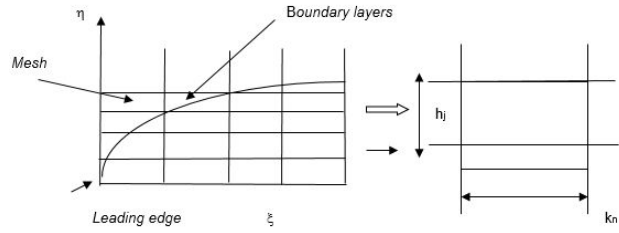


Fig. 2: Keller Box element and boundary layer mesh

where k_n and h_j denote the step distances in the ξ and η directions respectively.

If g_j^n denotes the value of any variable at (η_j, ξ^n) , then the variables and derivatives of Equations (22) - (29) at $(\eta_{j-1/2}, \xi^{n-1/2})$ are replaced by:

$$g_{j-1/2}^{n-1/2} = \frac{1}{4} (g_j^n + g_{j-1}^n + g_j^{n-1} + g_{j-1}^{n-1}), \quad (33)$$

$$\left(\frac{\partial g}{\partial \eta} \right)_{j-1/2}^{n-1/2} = \frac{1}{2h_j} (g_j^n - g_{j-1}^n + g_j^{n-1} - g_{j-1}^{n-1}), \quad (34)$$

$$\left(\frac{\partial g}{\partial \xi} \right)_{j-1/2}^{n-1/2} = \frac{1}{2k_n} (g_j^n - g_{j-1}^n + g_j^{n-1} - g_{j-1}^{n-1}), \quad (35)$$

The finite-difference approximation of equations (22) - (29) for the mid-point $(\eta_{j-1/2}, \xi^n)$, below:

$$h_j^{-1} (f_j^n - f_{j-1}^n) = u_{j-1/2}^n, \quad (36)$$

$$h_j^{-1} (u_j^n - u_{j-1}^n) = v_{j-1/2}^n, \quad (37)$$

$$h_j^{-1} (g_j^n - g_{j-1}^n) = p_{j-1/2}^n, \quad (38)$$

$$h_j^{-1} (\theta_j^n - \theta_{j-1}^n) = t_{j-1/2}^n, \quad (39)$$

$$\begin{aligned} & (v_j - v_{j-1}) + (3 + \alpha) \frac{h_j}{4} [(f_j + f_{j-1})(v_j + v_{j-1})] \\ & - \frac{(2 + \alpha) h_j}{4} (u_j + u_{j-1})^2 + \xi (v_j + v_{j-1}) \\ & + \frac{We}{2} (v_j + v_{j-1})(v_j - v_{j-1}) + \frac{h_j}{2} ((s_j + s_{j-1}) + N(g_j + g_{j-1})) \\ & - \frac{Mh_j}{2} (u_j + u_{j-1}) - \frac{\alpha h_j}{2} f_{j-1/2}^{n-1} (v_j + v_{j-1}) \\ & + \frac{\alpha h_j}{2} v_{j-1/2}^{n-1} (f_j + f_{j-1}) = [R_1]_{j-1/2}^{n-1} \end{aligned} \quad (40)$$

$$\begin{aligned}
& \frac{1}{Pr} (t_j - t_{j-1}) + (3 + \alpha) \frac{h_j}{4} [(f_j + f_{j-1}) (t_j + t_{j-1})] \\
& + \xi (t_j + t_{j-1}) - \frac{\alpha h_j}{4} [(u_j + u_{j-1}) (s_j + s_{j-1})] \\
& + \frac{\alpha h_j}{2} s_{j-1/2}^{n-1} (u_j + u_{j-1}) - \frac{\alpha h_j}{2} u_{j-1/2}^{n-1} (s_j + s_{j-1}) \\
& - \frac{\alpha h_j}{2} f_{j-1/2}^{n-1} (t_j + t_{j-1}) + \frac{\alpha h_j}{2} t_{j-1/2}^{n-1} (f_j + f_{j-1}) = [R_2]_{j-1/2}^{n-1}
\end{aligned} \quad (41)$$

$$\begin{aligned}
& \frac{1}{Le} (p_j - p_{j-1}) + \frac{(3 + \alpha) h_j}{4} [(f_j + f_{j-1}) (p_j + p_{j-1})] \\
& + \xi (p_j + p_{j-1}) - \frac{\alpha h_j}{4} [(u_j + u_{j-1}) (g_j + g_{j-1})] \\
& + \frac{\alpha h_j}{2} s_{j-1/2}^{n-1} (u_j + u_{j-1}) + \frac{B}{Le} (t_j - t_{j-1}) \\
& - \frac{\alpha h_j}{2} u_{j-1/2}^{n-1} (g_j + g_{j-1}) - \frac{\alpha h_j}{2} f_{j-1/2}^{n-1} (p_j + p_{j-1}) \\
& + \frac{\alpha h_j}{2} p_{j-1/2}^{n-1} (f_j + f_{j-1}) = [R_3]_{j-1/2}^{n-1}
\end{aligned} \quad (42)$$

Where the following notation applies:

$$\alpha = \frac{\xi^{n-1/2}}{k_n}, B = \frac{Nt}{Nb} \quad (43)$$

$$\begin{aligned}
[R_1]_{j-1/2}^{n-1} &= -h_j \left[\left(\frac{v_j - v_{j-1}}{h_j} \right) + (1 - \alpha) (f_{j-1/2} v_{j-1/2}) \right. \\
& + We v_{j-1} v'_{j-1/2} + (2 - \alpha) (u_{j-1/2})^2 - M (u_{j-1/2}) \\
& \left. + (3f_{j-1/2} + \xi - \alpha) (v_{j-1/2}) + (s_{j-1/2} + Ng_{j-1/2}) \right] \quad (44)
\end{aligned}$$

$$\begin{aligned}
[R_2]_{j-1/2}^{n-1} &= -h_j \left[\frac{1}{Pr} \left(\frac{t_j - t_{j-1}}{h_j} \right) + \alpha (u_{j-1/2} s_{j-1/2}) \right. \\
& - Nb (p_{j-1/2} t_{j-1/2}) + (3f_{j-1/2} + \xi - \alpha) (t_{j-1/2}) \\
& \left. - Nt (t_{j-1/2})^2 \right] \quad (45)
\end{aligned}$$

$$\begin{aligned}
[R_3]_{j-1/2}^{n-1} &= -h_j \left[\frac{1}{Le} \left(\frac{p_j - p_{j-1}}{h_j} \right) + (3f_{j-1/2} + \xi - \alpha) (p_{j-1/2}) \right. \\
& \left. + \frac{B}{Le} \left(\frac{t_j - t_{j-1}}{h_j} \right) + \alpha (u_{j-1/2} g_{j-1/2}) \right] \quad (46)
\end{aligned}$$

The boundary conditions are

$$\begin{aligned}
f_0^n &= u_0^n = 0, \theta_0^n = 1, u_j^n = 0, v_j^n = 0, \theta_j^n = 0, \\
\varphi_0^n &= 1, \varphi_j^n = 0
\end{aligned} \quad (47)$$

The emerging non-linear system of algebraic equations is *linearized* by means of Newton's method and then solved by the *block-elimination* method. The accuracy of computations is influenced by the number of mesh points in both directions. After experimenting with various grid sizes in the η -direction (radial coordinate) a larger number

of mesh points are selected whereas in the ξ direction (tangential coordinate) significantly less mesh points are utilized. η_{max} has been set at 12 and this defines a sufficiently large value at which the prescribed boundary conditions are satisfied. ξ_{max} is set at 1.0 for this flow domain. *Mesh independence* is therefore achieved in the present computations. The computer program of the algorithm is executed in MATLAB running on a PC.

If we assume f_{j-1}^{n-1} , u_{j-1}^{n-1} , v_{j-1}^{n-1} , p_{j-1}^{n-1} , s_{j-1}^{n-1} , t_{j-1}^{n-1} , to be known for $0 \leq j \leq J$, Eqs. (36) – (42) are a system of $6J+6$ equations for the solution of $5J+5$ unknowns f_j^n , u_j^n , v_j^n , p_j^n , s_j^n , t_j^n , $j = 0, 1, 2 \dots J$. This non-linear system of algebraic equations is linearized by means of Newton's method which then solved in a very efficient manner by using the Keller-box method, which has been used most efficiently by Cebeci and Bradshaw [54], taking the initial interaction with a given set of converged solutions at $\xi = \xi^n$. To initiate the process with $\xi = 0$, we first prescribe a set of guess profiles for the functions f, u, v, p, θ and t which are unconditionally convergent. These profiles are then employed in the Keller-box scheme with second-order accuracy to compute the correct solution step by step along the boundary layer. For a given ξ the iterative procedure is stopped to give the final velocity and temperature distribution when the difference in computing these functions in the next procedure become less than 10^{-5} , i.e., $|\delta f^i| \leq 10^{-5}$, where the superscript i denotes the number of iterations. For laminar flows the rate of convergence of the solutions of the equations (36)- (42) is quadratic provided the initial estimate to the desired solution is reasonably close to the final solution. Calculations are performed with four different $\Delta\eta$ spacings show that the rate of convergence of the solutions is quadratic in all cases for these initial profiles with typical iterations. The fact that Newton's method is used to to linearize the non-linear algebraic equations and that with proper initial guess ξ_n usually obtained from a solution at ξ_{n-1} , the rate of convergence of the solutions should be quadratic can be used to test the code for possible programming errors and to aid in the choice of $\Delta\xi$ spacings in the downstream direction. To study the effect of $\Delta\xi$ spacing on the rate of convergence of solutions, calculations were performed in the range $0 \leq \xi \leq 0.4$ with uniform $\Delta\xi$ spacings corresponding to 0.08, 0.04, 0.02 and 0.01. Except for the results obtained with $\Delta\xi = 0.08$, the rate of convergence of the solutions was essentially quadratic at each ξ station. In most laminar boundary layer flows, a step size of $\Delta y = 0.02$ to 0.04 is sufficient to provide accurate and comparable results. In fact in the present problem, we can even go up to $\Delta y = 0.1$ and still get accurate and comparable results. This particu-

lar value of ξ has also been used successfully by Merkin [45]. A uniform grid across the boundary is quite satisfactory for most laminar flow calculations, especially in laminar boundary layer. However, the Keller-box method is unique in which various spacing in both η and ξ directions can be used (Aldoss et al., [46]).

4 Validation of Keller Box Solutions

The present Keller box solutions have been validated for the special case of non-magnetic ($M=0$) Newtonian flow ($We = 0$) in the absence of thermal and partial slip ($S_f=S_T=0$). It is also the following reduced form:

$$f''' + ff'' - 2f'^2 + \theta + N\phi = \xi \left(f' \frac{\partial f'}{\partial \xi} - f'' \frac{\partial f}{\partial \xi} \right) \quad (48)$$

At $\eta = 0; f = 0; f' = 0, \theta = 1, \phi = 1$

At $\eta \rightarrow \infty : f' \rightarrow 0; \theta \rightarrow 0; \phi \rightarrow 0$

The energy equation (16) is identical to that considered in Chamkha and Aly [49], Bejan [47] and Kuznetsov and Nield [48]. The comparison of solutions is documented in Table 1. Excellent correlation is achieved and confidence in the present solutions is therefore justifiably high.

5 Results and Discussion

Extensive computations have been conducted using the Keller box code to study the influence of the key thermo-physical parameters on velocity, temperature, skin friction and Nusselt number. These are visualized in Figs. 3a-c to Figs. 12a-c.

Figs 3a-c illustrate the influence of Weissenberg number (We) on velocity, temperature and concentration profiles. We arises only in the momentum Eqn. (15) in the mixed derivative $We f'' f'''$. Weissenberg number (We) measures the relative effects of viscosity to elasticity. Weissenberg number of zero corresponds to a purely Newtonian fluid, and infinite Weissenberg number corresponds to a purely elastic solid. Intermediate values correlate quite well with actual polymeric viscoelastic properties. With increasing We , there is a general decrease through the boundary layer in velocity magnitudes. The boundary layer flow is therefore decelerated as viscous effects are depleted since resistance to the flow is reduced.

The momentum boundary layer is therefore depleted with greater Weissenberg number. We note that in Fig. 3a the magnetic body force parameter, M , is set at unity

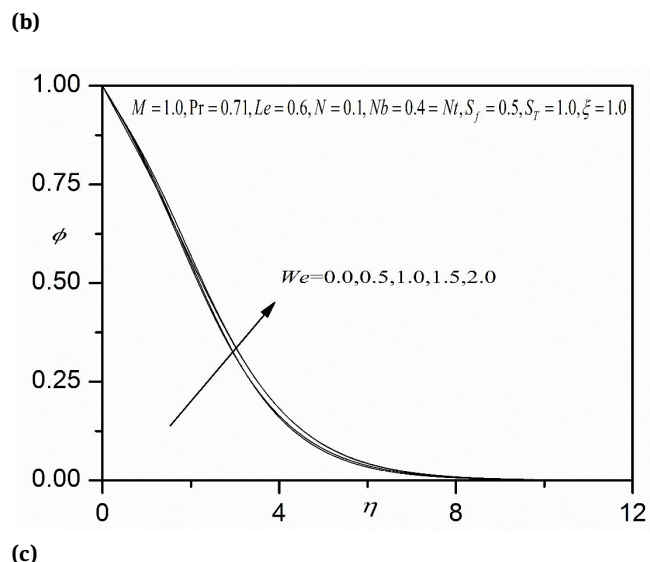
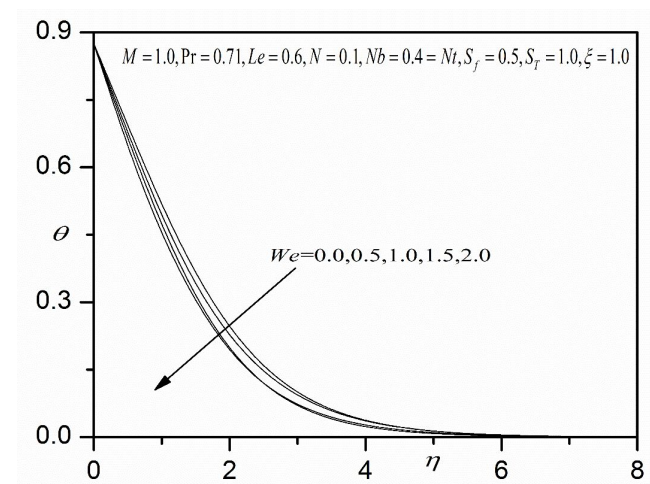
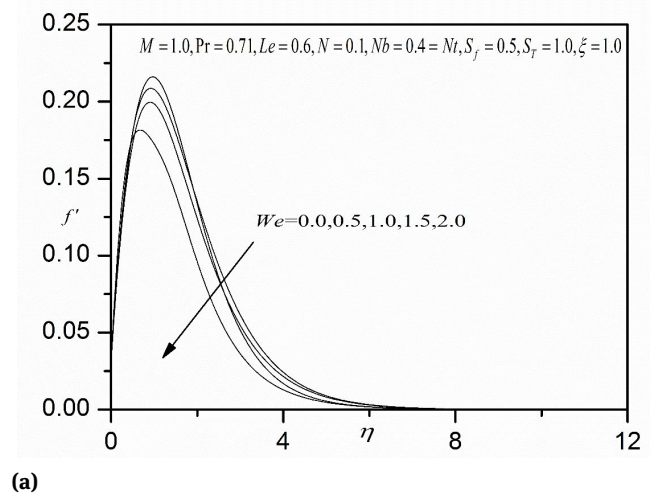


Fig. 3: (a) Effect of We on velocity profile; (b) Effect of We on temperature profile; (c) Effect of We on concentration profiles.

Table 1: Comparison of the Nusselt number for various values of Pr with $Le=10, N=Nb=Nt=10^{-5}, S_f=0, S_T=0$ and $M=0$

Pr	Bejan[47]	Kuznetsov and Nield [48]	Chamkha and Aly [49]	Present Work
1	0.401	0.401	0.40178	0.40181
10	0.465	0.463	0.4658	0.4656
100	0.490	0.481	0.49063	0.49066
1000	0.499	0.484	0.49739	0.49742

Table 2: Values of skin friction (Cf), Nusselt number (Nu) and Sherwood number (Sh) for different S_f, S_T and ξ

S_f	S_T	$\xi = 1.0$			$\xi = 2.0$			$\xi = 3.0$		
		Cf	Nu	Sh	Cf	Nu	Sh	Cf	Nu	Sh
0.0		0.6492	0.4174	0.1928	0.7343	0.4289	0.1920	0.7965	0.4404	0.1880
0.5	1.0	0.5847	0.4306	0.1926	0.6453	0.4423	0.1917	0.6822	0.4511	0.1873
1.0		0.5196	0.4438	0.1920	0.5570	0.4556	0.1915	0.5713	0.4676	0.1836
1.5		0.4535	0.4569	0.1917	0.4673	0.4738	0.1873	0.4623	0.4830	0.1808
2.0		0.3863	0.4701	0.1913	0.3769	0.4869	0.1869	0.3503	0.5028	0.1715
	0.0	0.6566	0.5079	0.1664	0.7198	0.5566	0.1379	0.7689	0.5507	0.1481
	1.0	0.5847	0.4306	0.1926	0.6453	0.4423	0.1917	0.6822	0.4511	0.1873
0.5	2.0	0.5114	0.3527	0.2173	0.5657	0.3632	0.2186	0.5978	0.3722	0.2140
	3.0	0.4355	0.2784	0.2376	0.4829	0.2894	0.2388	0.5099	0.2986	0.2328
	4.0	0.3547	0.2158	0.2459	0.3961	0.2174	0.2549	0.4180	0.2229	0.2527

Table 3: Values of skin friction (Cf), Nusselt number (Nu) and Sherwood number (Sh) for different Nb, Nt, M and We

Nb	Nt	M	$We = 0.0$			$We = 1.0$					
			Cf	Nu	Sh	Cf	Nu	Sh	Cf	Nu	Sh
0.5			0.5761	0.4164	0.2443	0.5899	0.4241	0.2468	0.6922	0.4550	0.2472
0.8	0.4		0.5760	0.4167	0.3221	0.5889	0.4207	0.3227	0.6833	0.4442	0.3317
1.2		0.5758	0.4167	0.3552	0.5876	0.4178	0.3642	0.6738	0.4187	0.3814	
1.6		0.5756	0.4157	0.3767	0.5863	0.4151	0.3845	0.6625	0.4135	0.4011	
2.0		0.5751	0.4145	0.3891	0.5852	0.4132	0.3962	0.6531	0.4106	0.4118	
	0.5	1.0	0.5860	0.4170	0.1267	0.5903	0.4260	0.1324	0.6923	0.4624	0.1869
	0.8	0.5862	0.4182	-0.0710	0.5906	0.4279	-0.0604	0.6926	0.4856	-0.0086	
	1.2	0.5863	0.4221	-0.3370	0.5909	0.4328	-0.3278	0.6929	0.5197	-0.3093	
	1.6	0.5865	0.4238	-0.6221	0.5911	0.4410	-0.6161	0.6928	0.5579	-0.6055	
0.4	2.0	0.5867	0.4246	-0.9439	0.5914	0.4535	-0.9372	0.6925	0.6010	-0.0907	
	0.0	0.7662	0.4908	0.2874	0.7436	0.4819	0.2825	0.7515	0.4751	0.2831	
	1.0	0.5961	0.4364	0.2443	0.5899	0.4241	0.2468	0.6922	0.4550	0.2472	
	2.0	0.4843	0.4181	0.1999	0.5016	0.3892	0.2193	0.6661	0.4324	0.2318	
	3.0	0.4093	0.3514	0.1936	0.4458	0.3607	0.1999	0.6319	0.4318	0.2173	

implying that the Lorentzian magnetic drag and viscous hydrodynamic force are of the same magnitude. Fig. 3b shows that a consistent elevation is computed in temperature of the viscoelastic fluid with greater values of Weissenberg number, We . The deceleration in the flow aids in momentum development which also assists in thermal diffusion, leading to heating of the boundary layer. Thermal boundary layer thickness is therefore *reduced* with increasing We values i.e. decreasing viscosity and increasing elastic effects. Effectively therefore Newtonian fluids ($We = 0$) achieve lower velocities and temperatures than Williamson fluids. An increase in Weissenberg param-

eter however increases nano-particle concentration magnitudes throughout the boundary layer, although the reduction is relatively weak. Thermal and nanoparticle concentration boundary layer thickness are both suppressed with greater viscoelasticity of the nanofluid.

Figs. 4a-c present the evolution in velocity, temperature and concentration functions with a variation in magnetic body force parameter (M). The radial magnetic field generates a transverse retarding body force. This decelerates the boundary layer flow and velocities are therefore reduced as observed in Fig. 4a. The momentum development in the viscoelastic coating can therefore be con-

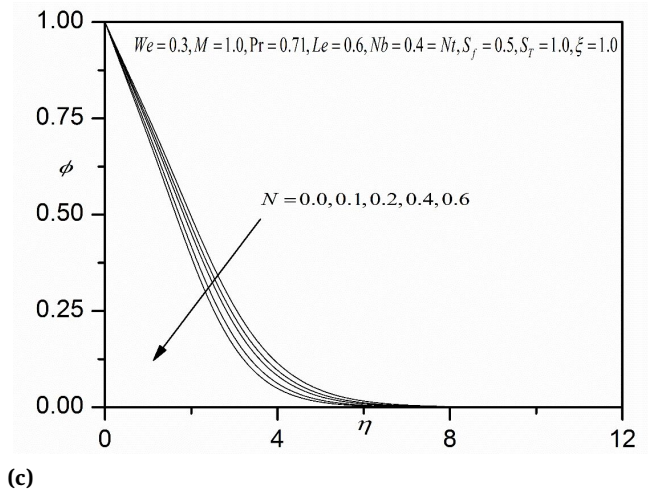
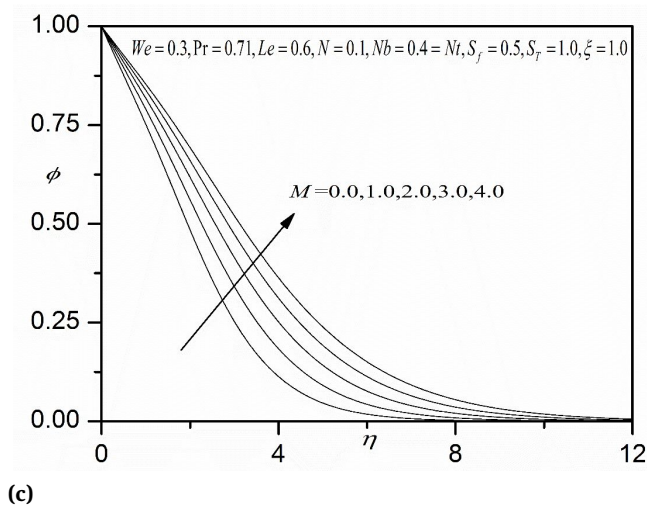
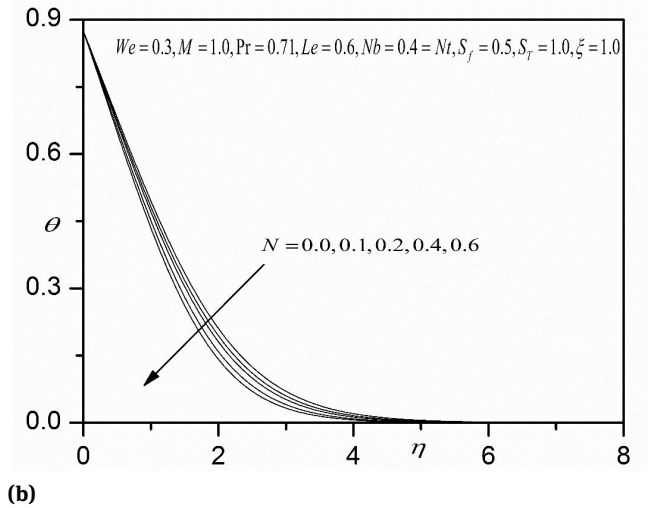
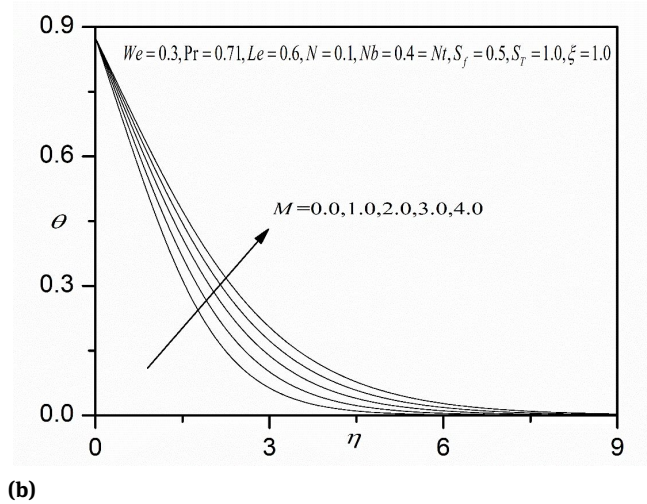
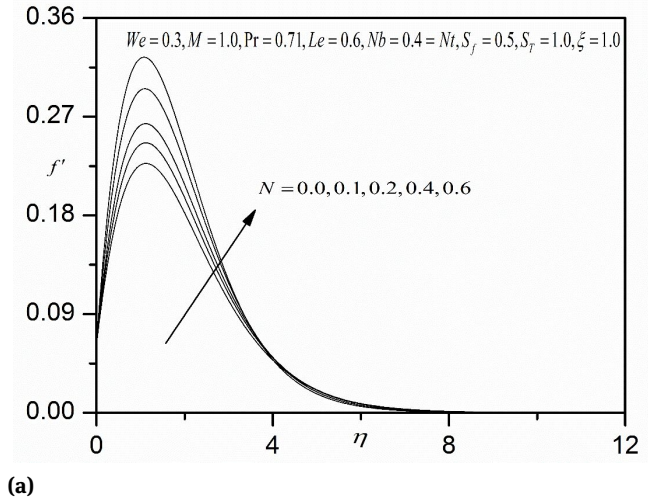
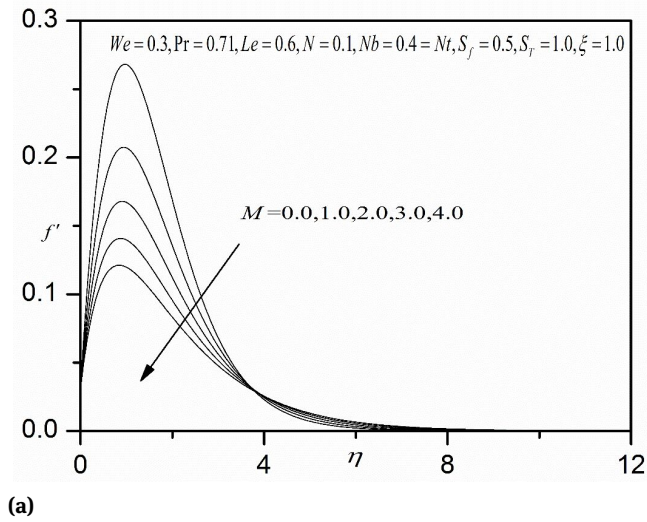
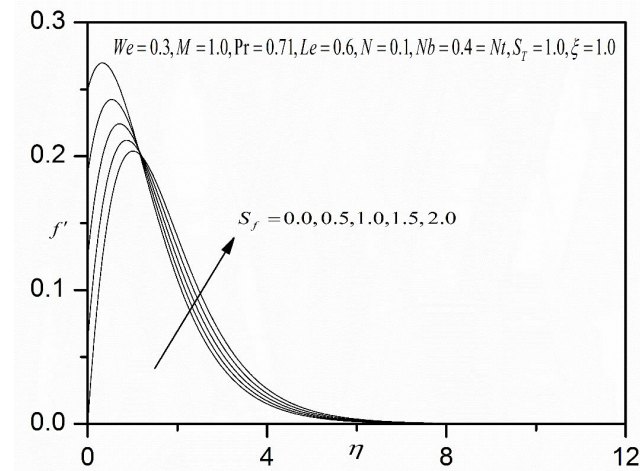
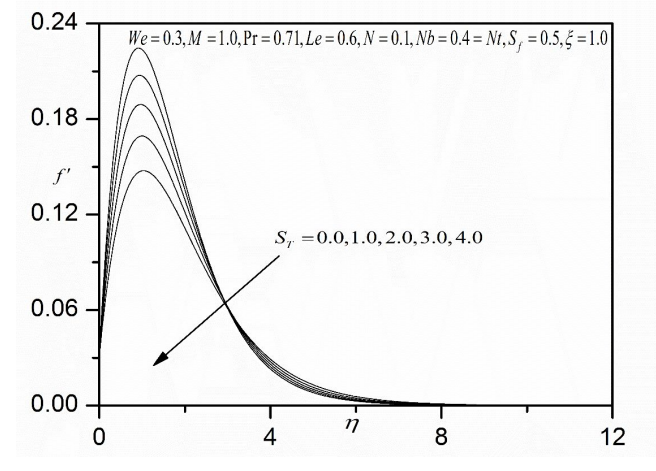


Fig. 4: (a) Effect of M on velocity profile; (b) Effect of M on temperature profile; (c) Effect of M on concentration profiles.

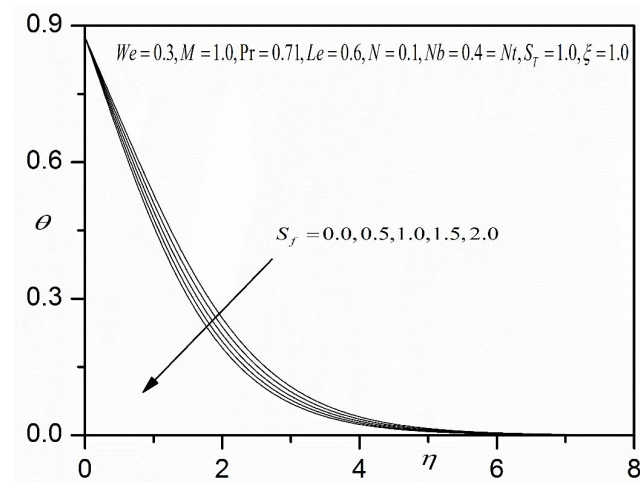
Fig. 5: (a) Effect of N on velocity profile; (b) Effect of N on temperature profile; (c) Effect of N on concentration profiles.



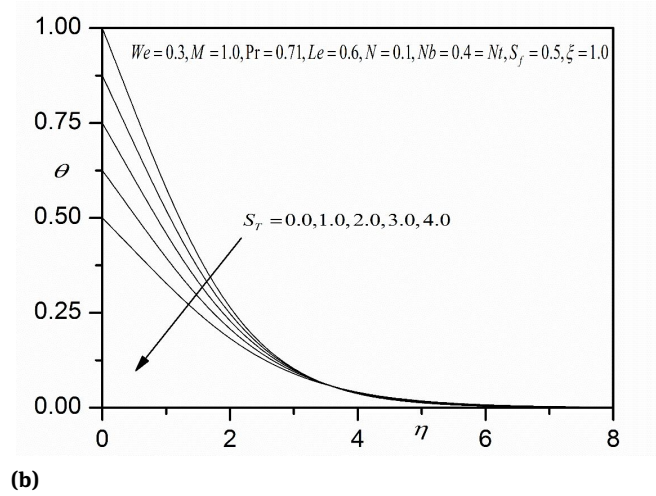
(a)



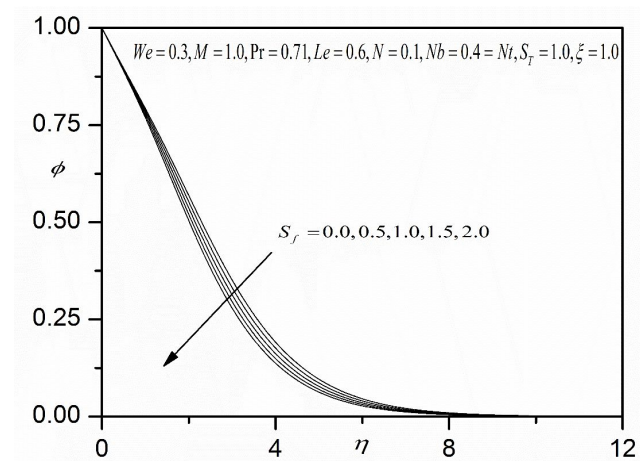
(a)



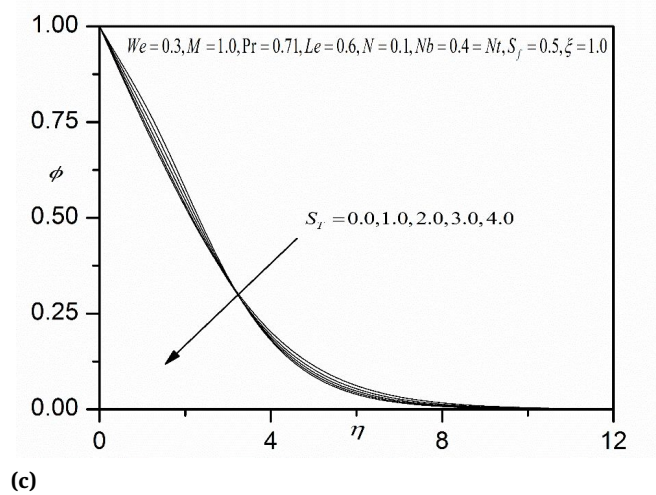
(b)



(b)



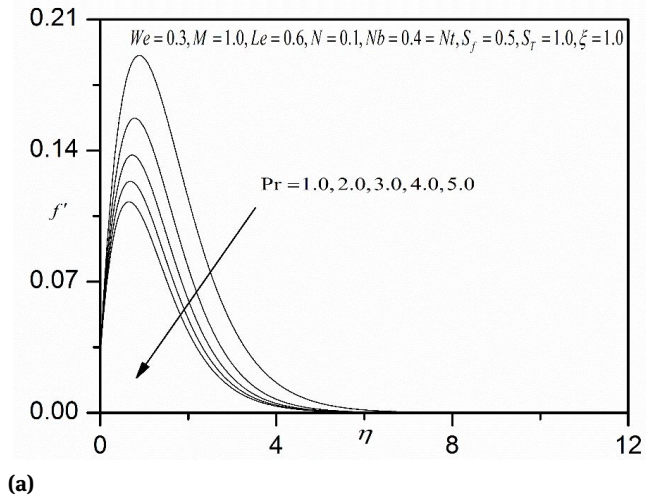
(c)



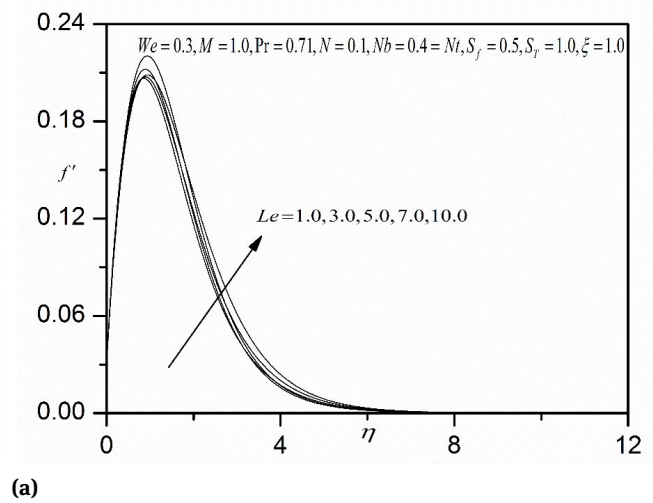
(c)

Fig. 6: (a) Effect of S_f on velocity profile; (b) Effect of S_f on temperature profile; (c) Effect of S_f on concentration profiles.

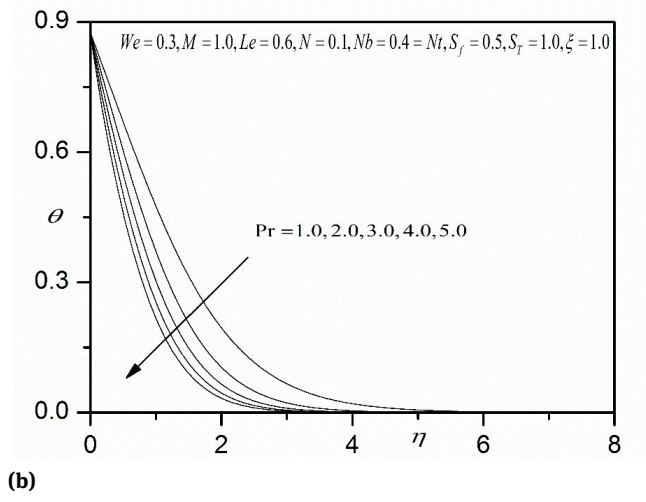
Fig. 7: (a) Effect of S_T on velocity profile; (b) Effect of S_T on temperature profile; (c) Effect of S_T on concentration profiles.



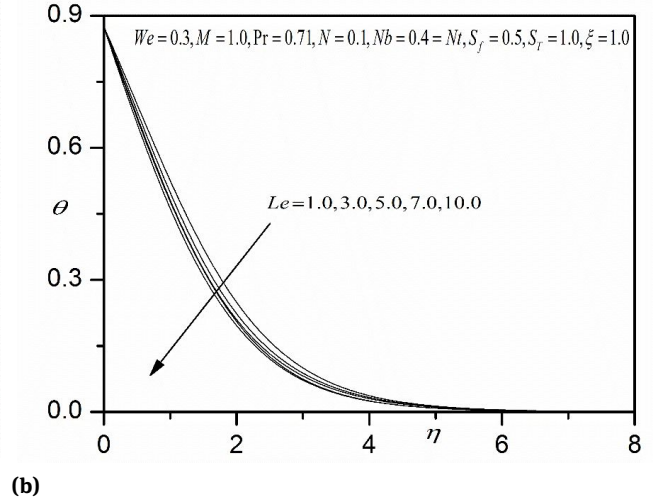
(a)



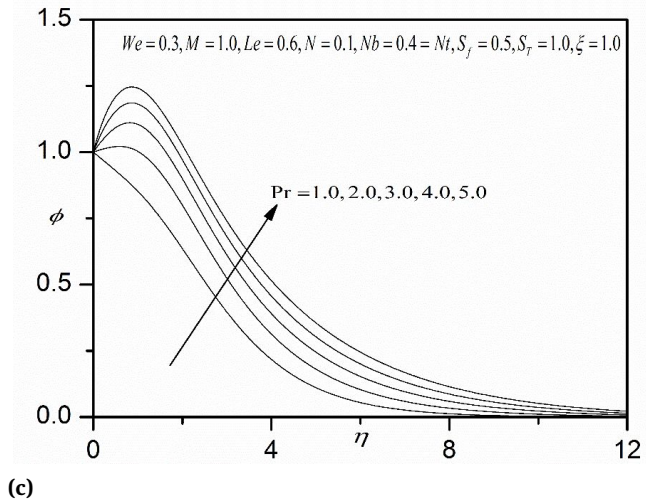
(a)



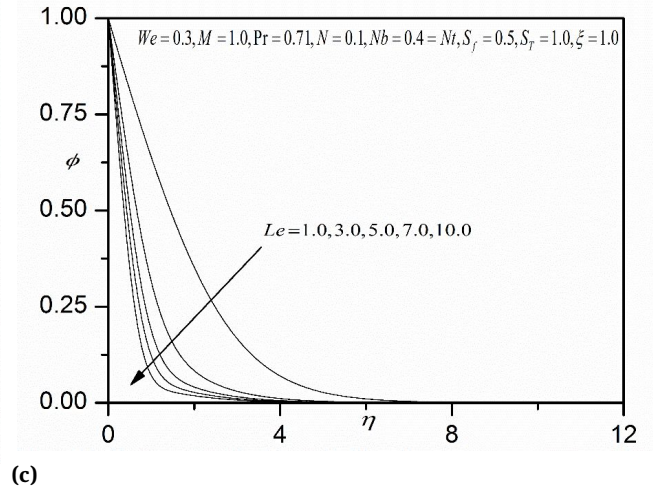
(b)



(b)



(c)



(c)

Fig. 8: (a) Effect of Pr on velocity profile; (b) Effect of Pr on temperature profile; (c) Effect of Pr on concentration profiles.

Fig. 9: (a) Effect of Le on velocity profile; (b) Effect of Le on temperature profile; (c) Effect of Le on concentration profiles.

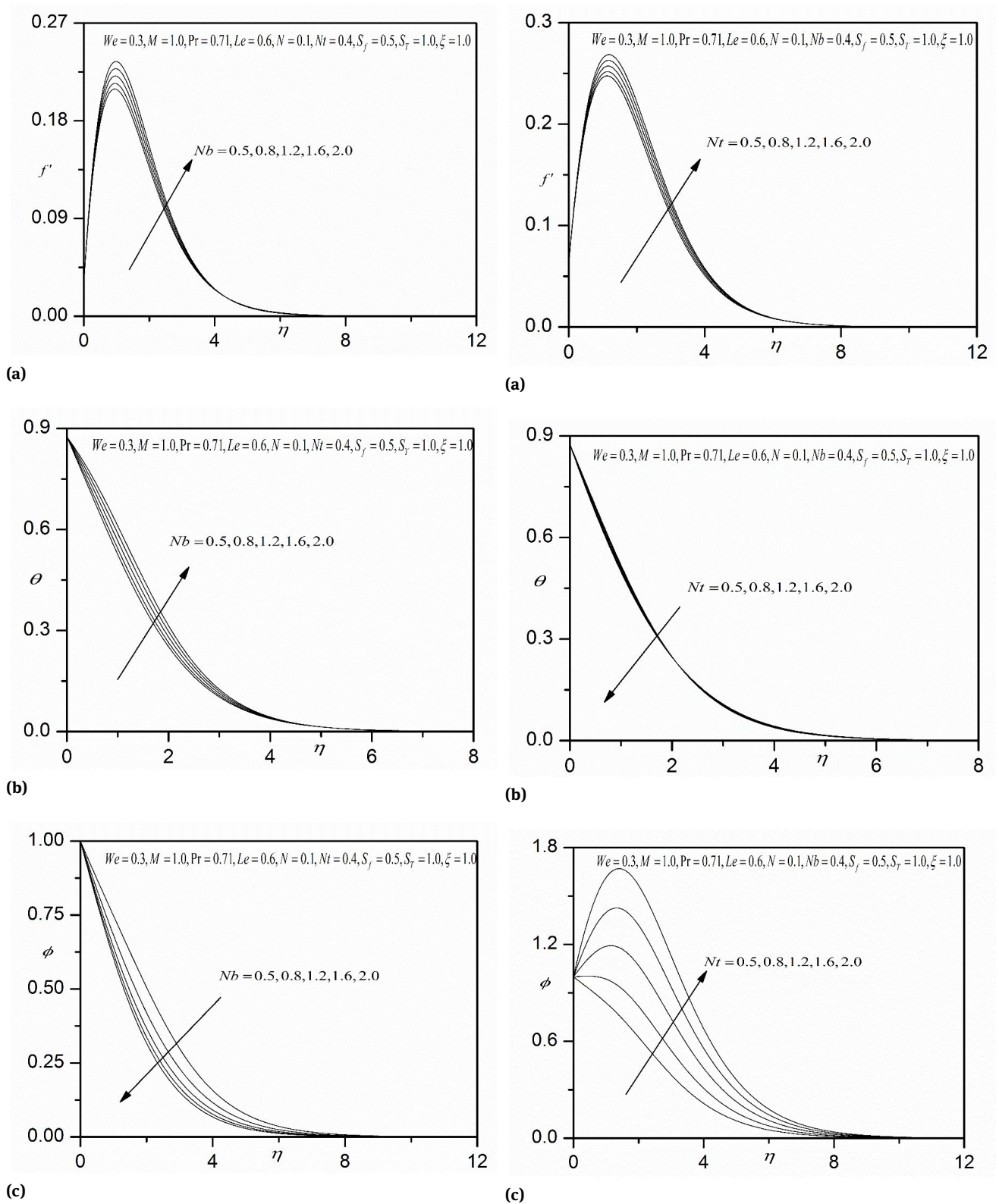


Fig. 10: (a) Effect of Nb on velocity profile; (b) Effect of Nb on temperature profile; (c) Effect of Nb on concentration profiles.

Fig. 11: (a) Effect of Nr on velocity profile; (b) Effect of Nr on temperature profile; (c) Effect of Nr on concentration profiles.

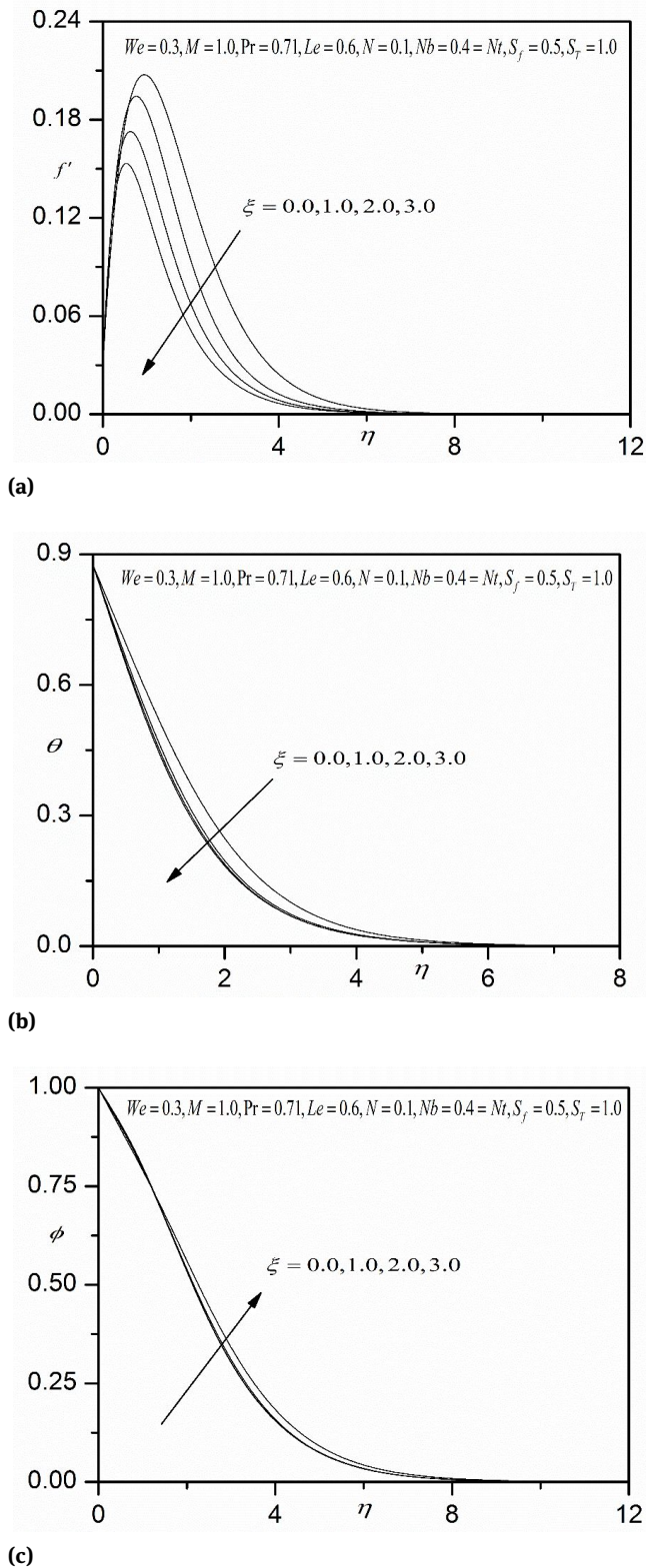


Fig. 12: (a) Effect of ξ on velocity profile; (b) Effect of ξ on temperature profile; (c) Effect of ξ on concentration profiles.

trolled using a radial magnetic field. The effect is prominent throughout the boundary layer from the plate surface to the free stream. Momentum (hydrodynamic) boundary layer thickness is therefore increased with greater magnetic field. Fig. 4b and 4c shows that both temperatures and nano-particle concentrations are strongly enhanced with greater magnetic parameter. The excess work expended in dragging the polymer against the action of the magnetic field is dissipated as thermal energy (heat). This energizes the boundary layer and increases thermal boundary layer thickness. Again the influence of magnetic field is sustained throughout the entire boundary layer domain. This energizes the boundary layer since the kinetic energy is dissipated as thermal energy, and this further serves to agitate improved species diffusion. As a result both thermal and nano-particle (species) concentration boundary layer thicknesses are increased. These results concur with other investigations of magnetic non-Newtonian heat transfer including Kasim *et al.* [50] and Megahed [51].

Figs. 5a-c exhibit the profiles for velocity, temperature and concentration, respectively with increasing buoyancy ratio parameter, N . In general, increases in the value of N have the prevalent to cause more induced flow along the plate surface. This behaviour in the flow velocity increases in the fluid temperature and volume fraction species as well as slight decreased in the thermal and species boundary layers thickness as N increases.

Figs. 6a-b illustrate the impact of the momentum (hydrodynamic) slip parameter (S_f) on the velocity, temperature and nano-particle concentration distributions. Near the plate surface there is a distinct elevation in velocity with greater momentum slip effect. S_f features in the velocity wall boundary condition in Eqn. (18) i.e. $f'(0) = S_f$ $f''(0)$. With increasing values of S_f the polymer slips i.e. shears more easily against the plate surface. This boosts momentum in the boundary layer and accelerates the flow (Fig. 6a). However, with progressive penetration into the boundary layer, this effect is reversed (as expected) and the flow is decelerated with greater momentum slip further from the plate surface. The velocity slip effect is strongest at the plate surface ($\eta = 0$). A similar observation has been made by Yarin and Graham [52] and also by Jamil and Khan [53]. The momentum slip effect is prominent and substantially modifies the velocity growth structure. Temperature is conversely reduced consistently throughout the boundary layer with greater momentum slip. The viscoelastic polymer is therefore cooled with wall momentum slip and this reduces thermal boundary layer thickness. The implication is therefore that with an absence of velocity slip in mathematical models, temperature is over-

predicted (the maximum value corresponds to $S_f = 0$). It is also apparent from Fig. 6c that nanoparticle concentration is enhanced with greater Velocity slip effect. Momentum boundary layer thickness is therefore reduced whereas thermal and species boundary layer thickness are enlarged. It is therefore important in more realistic simulations of nanofluid enrobing flows and polymer coating dynamics to incorporate wall slip effects.

Figs. 7a-c present the response in velocity, temperature and nano-particle concentration distributions to a modification in the thermal jump (slip) parameter (S_T). A marked depletion in velocity (Fig. 7a) accompanies an increase in thermal slip effect and this trend is sustained throughout the boundary layer. The thermal slip parameter indirectly influences the momentum field via coupling to the energy equation (thermal slip is only simulated in the wall thermal boundary condition in Eqn. 18). With greater thermal slip, there is also a very profound depletion in temperature at the plate surface and in close proximity to it (Fig. 7b). However, this effect weakens considerably with further distance from the plate surface and is effectively eliminated before reaching the free stream. Temperature profiles decay from a maximum at the plate surface to the free stream. It is also apparent from Fig. 7c that nanoparticle concentration is reduced with greater thermal slip effect. All profiles converge at a large value of transverse coordinate, again showing that a sufficiently large infinity boundary condition has been utilized in the numerical computations. Again the absence of thermal slip achieves higher temperatures indicating that without this modification in the thermal boundary condition at the wall (plate surface) the temperature is over-predicted, which can be critical to heat treatment of polymeric coatings [54]. Evidently the non-trivial responses computed in Figs. 7a-c further emphasize the need to incorporate thermal slip effects in realistic nanofluid enrobing flows.

Figs. 8a-c depict the evolution in velocity, temperature and nanoparticle concentration characteristics with transverse coordinate i.e. normal to the plate surface for various Prandtl numbers, Pr . Relatively high values of Pr are considered since these physically correspond to industrial polymers [53]. Prandtl number embodies the ratio of momentum diffusivity to thermal diffusivity in the boundary layer regime. It also represents the ratio of the product of specific heat capacity and dynamic viscosity, to the fluid thermal conductivity. For polymers momentum diffusion rate greatly exceeds thermal diffusion rate. The low values of thermal conductivity in most polymers also result in a high Prandtl number. With increasing Pr from 1 to 5 there is evidently a substantial deceleration in boundary layer flow i.e. a thickening in the momentum boundary

layer (Fig. 4a). The effect is most prominent close to the plate surface. Also Fig. 4b shows that with greater Prandtl number the temperature values are strongly decreased throughout the boundary layer transverse to the plate surface. Thermal boundary layer thickness is therefore significantly reduced. Inspection of Fig. 4c reveals that increasing Prandtl number strongly elevates the nano-particle concentration magnitudes. In fact a concentration overshoot is induced near the plate surface. Therefore while thermal transport is reduced with greater Prandtl number, species diffusion is encouraged and nano-particle concentration boundary layer thickness grows. The asymptotically smooth profiles in the free stream (high η values) confirm that an adequately large infinity boundary condition has been imposed in the Keller box numerical code.

Figs. 9a-c illustrate the evolution of velocity, temperature and concentration functions with a variation in the Lewis number, is depicted. Lewis number is the ratio of thermal diffusivity to mass (nano-particle) species diffusivity. $Le = 1$ which physically implies that thermal diffusivity of the nanofluid and species diffusivity of the nanoparticles are the same and both boundary layer thicknesses are equivalent. For $Le < 1$, mass diffusivity exceeds thermal diffusivity and vice versa for $Le > 1$. Both cases are examined in Figs. 9a-9c. In Fig. 9a, a consistently weak decrease in velocity accompanies an increase in Lewis number. Momentum boundary layer thickness is therefore increased with greater Lewis number. This is sustained throughout the boundary layer. Fig. 9b shows that increasing Lewis number also depresses the temperature magnitudes and therefore reduces thermal boundary layer thickness. Therefore judicious selection of nano-particles during doping of polymers has a pronounced influence on velocity (momentum) and thermal characteristics in enrobing flow, since mass diffusivity is dependent on the nature of nano-particle species in the base fluid. Fig 9c demonstrates that a more dramatic depression in nano-particle concentration results from an increase in Lewis number over the same range as Figs. 9a,b. The concentration profile evolves from approximately linear decay to strongly parabolic decay with increment in Lewis number.

Figs. 10a-c depict the response in velocity, temperature and concentration functions to a variation in the Brownian motion parameter (Nb). Increasing Brownian motion parameter physically correlates with *smaller nanoparticle diameters*. Smaller values of Nb corresponding to larger nanoparticles, and imply that surface area is reduced which in turn decreases thermal conduction heat transfer to the plate surface. This coupled with enhanced macro-convection within the nanofluid energizes the boundary layer and accelerates the flow as observed

in Fig. 10a. Similarly the energization of the boundary layer elevates thermal energy which increases temperature in the viscoelastic nanofluid. Fig. 10c however indicates that the contrary response is computed in the nanoparticle concentration field. With greater Brownian motion number species diffusion is suppressed. Effectively therefore momentum and nanoparticle concentration boundary layer thickness is decreased whereas thermal boundary layer thickness is increased with higher Brownian motion parameter values.

Figs. 11a-c illustrates the effect of the thermophoresis parameter (Nt) on the velocity, temperature and concentration distributions, respectively. Thermophoretic migration of nano-particles results in exacerbated transfer of heat from the nanofluid regime to the plate surface. This de-energizes the boundary layer and inhibits simultaneously the diffusion of momentum, manifesting in a reduction in velocity i.e. retardation in the boundary layer flow and increasing momentum (hydrodynamic) boundary layer thickness, as computed in Fig. 11a. Temperature is similarly decreased with greater thermophoresis parameter (Fig. 11b). Conversely there is a substantial enhancement in nano-particle concentration (and species boundary layer thickness) with greater Nt values. Similar observations have been made by Kuznetsov and Nield [16] and Ferdows *et al.* [25] for respectively, both non-conducting Newtonian and electrically-conducting Newtonian flows.

Figs. 12a-c present the distributions for velocity, temperature and concentration fields with stream wise coordinate ξ , for the viscoelastic nanofluid flow. Increasing ξ values correspond to progression around the periphery of the vertical plate, from the leading edge ($\xi = 0$). As ξ increases, there is a weak deceleration in the flow (Fig. 12a), which is strongest nearer the plate surface and decays with distance into the free stream. Conversely there is a weak elevation in temperatures (Fig. 12b) and nano-particle concentration magnitudes (Fig. 12c) with increasing stream wise coordinate.

Table 2 illustrate the skin friction, Nusselt number and Sherwood number distributions with various values of momentum slip parameter (S_f) and thermal slip effect (S_T). A marked depreciation in skin friction and Sherwood number is observed with greater momentum slip. Conversely a strong elevation in Nusselt number is generated with greater momentum slip effect. The momentum slip effect is consistent for all values of stream wise parameter (ξ). The influence of momentum (hydrodynamic) slip is non-trivial and demonstrates that a sizeable modification in surface thermo-fluid characteristics is induced with slip and indeed that the methodology employed to simulate it quite realistically simulates real macroscopic effects of certain

molecular phenomena at polymer/solid interfaces. Both skin friction and Nusselt number are strongly reduced and Sherwood number is enhanced with an increase thermal slip (S_T). The boundary layer is therefore decelerated and heated with stronger thermal slip. With thermal slip absent therefore the skin friction is maximized at the plate surface. The inclusion of thermal slip, which is encountered in various slippy polymer flows, is therefore important in more physically realistic simulations.

Tables 3 presents the influence of magnetic parameter (M), Brownian motion parameter (Nb) and thermophoresis parameter (Nt), on skin friction, Nusselt number and Sherwood number, along with a variation in the Weissenberg number (We). A significant depletion is caused in skin friction with greater magnetic field, which corresponds to a retardation of the boundary layer flow. The maximum skin friction therefore is achieved only in the absence of a radial magnetic field i.e. $M = 0$. For $M < 1$, the magnetic body force is exceeded by the viscous hydrodynamic force in the regime. For $M > 1$ the contrary is the case. The reduction in Nusselt number with greater M values implies that the transfer of heat from the boundary layer to the wall (plate surface) is reduced. This physically indicates therefore that greater heat is conveyed away from the plate surface to the fluid which explains the higher temperatures associated with strong magnetic field in the earlier computations. Magnetic field is therefore a potent mechanism for controlling thermal and velocity characteristics in electrically-conducting polymer dynamics. With increasing Brownian motion parameter Nb , the skin friction is generally decreased, whereas heat transfer rate is decreased. Mass transfer rate is however increased with increasing Brownian motion parameter Nb . With increasing thermophoretic parameter Nt , the skin friction is slightly increased, whereas heat transfer rate is increased Mass transfer rate is however decreased with increasing thermophoretic parameter Nt . Increasing Weissenberg number (We) enhances skin friction, heat transfer rate (Nusselt number) and mass transfer rate (Sherwood number) and furthermore provide benchmarks against which other researchers may validate extensions of the present model.

6 Conclusions

A theoretical study has been conducted to simulate the viscoelastic nanofluid boundary layer flow in enrobing processes from a vertical plate with Partial slip effect using the Buonjornio formulation. The transformed momentum, heat and species boundary layer equations have

been solved computationally with Keller's finite difference method. The present study has shown that:

(i) Increasing Weissenberg number accelerates the near-wall flow and also increases temperatures (i.e. reduces Nusselt number).

(ii) Increasing Prandtl number retards the flow and also decreases temperatures and nano-particle concentration values.

(iii) Increasing stream wise coordinate decelerates the flow whereas it enhances temperatures and species (nano-particle) concentrations.

(iv) Increasing velocity slip strongly enhances velocities and reduces temperatures and nano-particle concentrations.

(v) Increasing thermal slip strongly reduces velocities, temperatures and nano-particle concentrations.

(vi) Increasing Brownian motion accelerates the flow and enhances temperatures whereas it reduces nanoparticle concentration boundary layer thickness.

(vii) Increasing thermophoretic parameter increasing momentum (hydrodynamic) boundary layer thickness and nanoparticle boundary layer thickness whereas it reduces thermal boundary layer thickness.

Acknowledgement: The authors appreciate the constructive comments of the reviewers which led to definite improvement in the paper. The first three authors are thankful to the management of Madanapalle Institute of Technology & Science, Madanapalle for providing research facilities in the campus.

Nomenclature

B_0 constant magnetic field (Tesla)

c_p specific heat at constant pressure (J/kg K)

C dimensional concentration

C_f skin friction coefficient

D_B Brownian diffusion coefficient (m^2/s)

D_T thermophoretic diffusion coefficient (m^2/s)

f non-dimensional stream function

Gr Grashof number

G acceleration due to gravity (m/s^2)

Le Lewis number

M magnetic field parameter

Nb Brownian motion parameter

Nt thermophoresis parameter

Nu local Nusselt number

Pr Prandtl number

S_f non-dimensional velocity slip parameter

S_T thermal slip (jump) parameter

T temperature (K)

u, v non-dimensional velocity components along the x - and y - directions, respectively (m/s)

We Weissenberg (viscoelasticity) number

x stream wise coordinate (m)

y transverse coordinate (m)

Greek symbols

α thermal diffusivity (m^2/s)

β coefficient of thermal expansion ($^{\circ}C^{-1}$)

η dimensionless transverse coordinate

ν kinematic viscosity (m^2/s)

θ non-dimensional temperature

ρ density of nanofluids ($Kg\ m^{-3}$)

σ electrical conductivity of nanofluid

ξ dimensionless stream wise coordinate

ψ dimensionless stream function

Γ time-dependent material constant

Subscripts

w conditions on the wall

∞ free stream conditions

References

- [1] Rojas JA, Santos K (2011) Magnetic nanophases of iron oxide embedded in polymer. Effects of magneto-hydrodynamic treatment of pure and wastewater, 5th Latin American Congress on Biomedical Engineering CLAIB 2011 May 16-21, 2011, Habana, Cuba.
- [2] Yonemura H, Takata M, Yamada S (2014) Magnetic field effects on photoelectrochemical reactions of electrodes modified with thin films consisting of conductive polymers, *J. Appl. Phys.* 53 01AD06
- [3] S. Rashidi, J. A. Esfahani, and M. Maskaniyan, Applications of magnetohydrodynamics in biological systems-a review on the numerical studies, *J. Magn. Magn. Mater.* 439, pp. 358-372, (2017). <https://doi.org/10.1016/j.jmmm.2017.05.014>
- [4] F. Ali, N. A. Sheikh, I. Khan, and M. Saqib, Magnetic field effect on blood flow of Casson fluid in axisymmetric cylindrical tube: A fractional model, *J. Magn. Magn. Mater.* 423, 327- 336, 2017. <https://doi.org/10.1016/j.jmmm.2016.09.125>
- [5] A. Rahbari, M. Fakour, A. Hamzehnezhad, M. A. Vakilabadi, and D. D. Ganji, Heat transfer and fluid flow of blood with nanoparticles through porous vessels in a magnetic field: A quasi-one dimensional analytical approach, *Math. Biosci.* 283, 38-47, 2017. <https://doi.org/10.1016/j.mbs.2016.11.009>
- [6] I. A. Mirza, M. Abdulhameed, and S. Shafie, Magnetohydrodynamic approach of non-Newtonian blood flow with magnetic

- particles in stenosed artery, *Appl. Math. Mech.* 38(3), 379–392, 2017. <https://doi.org/10.1007/s10483-017-2172-7>
- [7] Sharma A, Tyagi VV, Chen CR, Buddhi D (2009) Review on thermal energy storage with phase change materials and applications, *Renewable and Sustainable Energy Reviews.*, 13:318-345 <http://dx.doi.org/10.1016/j.rser.2007.10.005>
- [8] Choi SUS, Eastman JA (1995) Enhancing thermal conductivity of fluids with nanoparticles, ASME International Mechanical Engineering Congress & Exposition, San Francisco, USA, 66:99-105.
- [9] Choi S (1995) Enhancing thermal conductivity of fluids with nanoparticles ASME-Publ. Fluids Engineering Division., 231:99–106
- [10] Buongiorno J (2016) Convective transport in nanofluids, *ASME J. Heat Trans.*, 128:240–250 <http://dx.doi.org/10.1115/1.2150834>
- [11] Noghrehabadi A, Pourrajab R, Ghalambaz M (2012) Effect of partial slip boundary condition on the flow and heat transfer of nanofluids past stretching sheet prescribed constant wall temperature, *Int. J. Thermal Sci.*, 54:253–261 <http://dx.doi.org/10.1016/j.ijthermalsci.2011.11.017>
- [12] Khan WA, Pop I (2010) Boundary layer flow of a nanofluid past a stretching sheet, *Int. J. Heat Mass Transfer.*, 53:2477–2483 <http://dx.doi.org/10.1016/j.ijheatmasstransfer.2010.01.032>
- [13] Uddin MJ, Khan WA, Ismail AIM, Bég OA (2016) Computational study of three-dimensional stagnation point nanofluid bio-convection flow on a moving surface with anisotropic slip and thermal jump effect, *ASME J. Heat Transfer.*, 138(10), 7 pages <http://dx.doi.org/10.1115/1.4033581>
- [14] M.J Uddin, O. Anwar Bég, and Ahmad Izani Ismail. "Radiative Convective Nanofluid Flow Past a Stretching/Shrinking Sheet with Slip Effects", *Journal of Thermophysics and Heat Transfer*, Vol. 29, No. 3 (2015), pp. 513-523. <https://doi.org/10.2514/1.T4372>
- [15] Kuznetsov AV, Nield DA (2010) Natural convective boundary-layer flow of a nanofluid past a vertical plate, *Int. J. Thermal Sciences.*, 49(2):243-247 <http://dx.doi.org/10.1016/j.ijthermalsci.2009.07.015>
- [16] Kuznetsov AV, Nield DA (2014) Natural convective boundary layer flow of a nanofluid past a vertical plate: a revised model, *Int. J. Thermal Sciences.*, 77:126–129 <http://dx.doi.org/10.1016/j.ijthermalsci.2013.10.007>
- [17] Malik MY, Naseer M, Nadeem S, Abdul R (2014) The boundary layer flow of Casson nanofluid over a vertical exponentially stretching cylinder, *Appl Nanosci.*, 4:869–873 <http://dx.doi.org/10.1007/s13204-013-0267-0>
- [18] F. Ali, M. Gohar, and I. Khan, *J. Mol. Liq.* 223, 412 (2016).
- [19] M. Muthamilselvan, DH. Doh, Mixed convection of heat generating nanofluid in a lid-driven cavity with uniform and non-uniform heating of bottom wall, *Applied Mathematical Modelling* 38 (2014) 3164–3174
- [20] M Muthamilselvan and SS Kumar, Impact of aspect ratio on a nanofluid-saturated porous enclosure, *Mechanics & Industry* Vol.18(5), 2017. <https://doi.org/10.1051/meca/2016026>
- [21] K. Das, P. R. Duari and P. Kumar Kundu, Nanofluid flow over an unsteady stretching surface in presence of thermal radiation, *Alexandria engineering journal*, 53 (2014), 737–745.
- [22] D. Pal, G. Mandal and K. Vajravelu, Flow and heat transfer of nanofluids at a stagnation point flow over a stretching/shrinking surface in a porous medium with thermal radiation, *Applied mathematics computations*, 238 (2014) 208–224.
- [23] B. K. Mahatha, R. Nandkeolyar, G. K. Mahto and P. Sibanda, Dissipative effects in hydromagnetic boundary layer nanofluid flow past a stretching sheet with Newtonian heating, *Journal of applied fluid mechanics*, 9 (2016) 1977-1989.
- [24] A.J. Chamkha, A. M. Rashad and E. AlMeshai. Melting effect on unsteady hydromagnetic flow of a nanofluid past a stretching sheet, *International journal of chemical reactor engineering*, 9 (2011) A113.
- [25] M. Ferdows, Md. Shakhaoath Khan, Md. Mahmud Alam and A. A. Afify, MHD boundary layer flow and heat transfer characteristics of a nanofluid over a stretching sheet, *Acta universitatis sapientiae, Mathematica*, 9 (2017) 140–161.
- [26] F.G. Awad, S.M.S. Ahamed, P. Sibanda and M. Khumalo. The effect of thermophoresis on unsteady oldroyd-B nanofluid flow over stretching surface, *PLoS ONE*, 10 (2015): e0135914.
- [27] Ahmed A. Afify, The influence of slip boundary condition on casson nanofluid flow over a stretching sheet in the presence of viscous dissipation and chemical reaction, *Hindawi mathematical problems in engineering*, 2017 (2017) 1-12.
- [28] Prasannakumara BC, Gireesha BJ, Gorla RSR, Krishnamurthy MR (2016) Effects of chemical reaction and nonlinear thermal radiation on Williamson nanofluid slip flow over a stretching sheet embedded in a porous medium, *J. Aerosp. Eng.*, 29(5) [http://dx.doi.org/10.1061/\(ASCE\)AS.1943-5525.0000578](http://dx.doi.org/10.1061/(ASCE)AS.1943-5525.0000578)
- [29] Khan NA, Khan H (2014) A Boundary layer flows of non-Newtonian Williamson fluid, *Nonlinear Engineering*, 3(2):107–115 <http://dx.doi.org/10.1515/nleng-2014-0002>
- [30] Bég OA, Keimanesh M, Rashidi MM, Davoodi M (2013) Multi-step DTM simulation of magneto-peristaltic flow of a conducting Williamson viscoelastic fluid, *Int. J. Appl. Math. Mech.*, 9(6):1-19
- [31] Rao KS, Rao PK (2014) Fully developed free convective flow of a Williamson fluid through a porous medium in a vertical channel, *Int. J. Conceptions on Computing and Information Technology*, 2:54-57
- [32] Dapra I, Scarpi G (2007) Perturbation solution for pulsatile flow of a non-Newtonian Williamson fluid in a rock fracture, *Int. J. Rock Mechanics and Mining Sciences*, 44:271–278
- [33] F Mabood, SM Ibrahim, G Lorenzini, E Lorenzini, Radiation effects on Williamson nanofluid flow over a heated surface with magnetohydrodynamics, *international journal of heat and technology*, vol. 35(1), 2017, pp. 196-204
- [34] P. B. Sampath Kumar, B. J Gireesha, R. S. R. Gorla, B.Mahanthesh, Magnetohydrodynamic Flow of Williamson Nanofluid Due to an Exponentially Stretching Surface in the Presence of Thermal Radiation and Chemical Reaction, *Journal of Nanofluids*, Vol. 6(2), 2017, pp. 264-272.
- [35] Y B Kho, A Hussanan, M K A Mohamed, N M Sarif, Z Ismail and M Z Salleh, Thermal radiation effect on MHD Flow and heat transfer analysis of Williamson nanofluid past over a stretching sheet with constant wall temperature, *IOP Conf. Series: Journal of Physics: Conf. Series* 890 (2017) 012034.
- [36] CH Amanulla, N Nagendra, M Suryanarayana Reddy, Numerical Simulations on Magnetohydrodynamic Non-Newtonian Nanofluid Flow over a Semi-Infinite Vertical Surface with Slip effects, *Journal of Nanofluids*, Vol. 7(4), pp. 718-730, 2018. [doi:10.1166/jon.2018.1499](https://doi.org/10.1166/jon.2018.1499)
- [37] CH Amanulla, N Nagendra, M Suryanarayana Reddy Numerical Study of Thermal and Momentum Slip Effects on MHD

- Williamson Nanofluid from an Isothermal Sphere, *Journal of Nanofluids*, vol. 6(6), pp. 1111-1126, 2017.
- [38] M.J. Uddin, O. Anwar Bég, N. Amran, A.I.MD. Ismail, Lie group analysis and numerical solutions for magneto-convective slip flow of nanofluid over a moving plate with Newtonian heating boundary condition, *Canadian Journal of Physics*, 2015, 93(12): 1501-1509, <https://doi.org/10.1139/cjp-2014-0601>
- [39] M. J. Uddin; O. Anwar Bég; and M. N. Uddin, Multiple Slips and Variable Transport Property Effect on Magnetohydrodynamic Dissipative Thermosolutal Convection in a Porous Medium, *Journal of Aerospace Engineering*, vol. 29(5), 2016.
- [40] M.J.Uddina, A Yasser, O.Anwar Bég M.N. Kabir, Numerical solutions for gyrotactic bioconvection in nanofluid-saturated porous media with Stefan blowing and multiple slip effects, *Computers & Mathematics with Applications* Volume 72, Issue 10, November 2016, Pages 2562-2581.
- [41] Keller, H.B., "A new difference method for parabolic problems", J. Bramble (Editor), *Numerical Methods for Partial Differential Equations*, Academic Press, New York, USA.1970.
- [42] CH. Amanulla, N. Nagendra, M. Surya Narayana Reddy, A. Subba Rao, O. Anwar Bég, *Mathematical Study Of Non-Newtonian Nanofluid Transport Phenomena From An Isothermal Sphere*, *Frontiers in Heat and Mass Transfer*,8.29, 2017.: <http://dx.doi.org/10.5098/hmt.8.29>
- [43] C.H. Amanulla, N. Nagendra, and M. Suryanarayana Reddy, Computational analysis of non-Newtonian boundary layer flow of nanofluid past a semi-infinite vertical plate with partial slip, *Nonlinear Engineering*, 7(1), pp. 29-43, 2017. <https://doi.org/10.1515/nleng-2017-0055>
- [44] A.S. Rao, C.H. Amanulla, N. Nagendra, M. Surya Narayana Reddy, O. Anwar Bég, Hydromagnetic non-Newtonian nanofluid transport phenomena from an isothermal vertical cone with partial slip: Aerospace nanomaterial enrobing simulation, pp.203–230, 2018. <https://doi.org/10.1002/htj.21299>
- [45] J.H.Merkin, Free convection boundary layer on an isothermal Horizontal cylinder. ASME/AICHE Heat Transfer Conference. August 9-11 St. Louis USA, 1976.
- [46] Aldoss, T.K., Ali, Y.D. and A-Nimr, M.A. MHD Mixed convection from a horizontal circular cylinder. *Numerical heat transfer, part A*. 30: 379-396, 1996.
- [47] Bejan A (1984) *Convection Heat Transfer*, John Wiley, New York
- [48] Kuznetsov AV, Nield DA (2010) Natural convective boundary-layer flow of a nanofluid past a vertical plate, *Int. J. Therm. Sci.*, 49:243–247
- [49] Chamkha AJ, Aly AM (2011) MHD free convection flow of a nanofluid past a vertical plate in the presence of heat generation or absorption effects, *Chemical Engineering Communications*, 198(3):425-441 <http://dx.doi.org/10.1080/00986445.2010.520232>
- [50] Kasim ARM, Mohammad NF, Anwar I, Shafie S (2013) MHD effect on convective boundary layer flow of a viscoelastic fluid embedded in porous medium with Newtonian heating, *Recent Advances in Mathematics*, 4:182-189
- [51] Megahed AM (2012) Variable viscosity and slip velocity effects on the flow and heat transfer of a power-law fluid over a non-linearly stretching surface with heat flux and thermal radiation, *Rheologica Acta*, 51(9):841–84
- [52] Yarin AL, Graham MD (1998) A model for slip at polymer/solid interfaces, *J. Rheol.*, 42(6):1491–1504
- [53] Jamil M, Khan NA (2011) Slip effects on fractional viscoelastic fluids, *Int. J. Differential Equations*, 2011(2011):1-19, Article ID 193813 <http://dx.doi.org/10.1155/2011/193813>
- [54] Aly AA (2015) Heat treatment of polymers: a review, *Int. J. Materials Chemistry and Physics*, 1(2):132-140.